Physicochem. Probl. Miner. Process., 54(1), 2018, 89-101

www.minproc.pwr.wroc.pl/journal/

Physicochemical Problems of Mineral Processing

ISSN 1643-1049

Received June 25, 2017; reviewed; accepted July 31, 2017

Molecular dynamics simulations study of nano bubble attachment at hydrophobic surfaces

Jiaqi Jin [1], Liem X. Dang [2], Jan D. Miller [1]

[1] University of Utah, Department of Metallurgical Engineering, 135 South 1460 East, Rm 412, Salt Lake City, UT 84112

[2] Physical Sciences Division, Pacific Northwest National Laboratory, 902 Battelle Boulevard, Richland, WA 99352

Corresponding author: jan.miller@utah.edu (Jan D. Miller)

Abstract: Bubble attachment phenomena are examined using Molecular Dynamics Simulations (MDS) for the first time. The simulation involves a nitrogen nano bubble containing 906 nitrogen molecules in a water phase with 74,000 water molecules at molybdenite surfaces. During a simulation period of 1 ns, film rupture and displacement occurs. The attached nanobubble at the hydrophobic molybdenite face surface results in a contact angle of about 90°. This spontaneous attachment is due to a "water exclusion zone" at the molybdenite face surface and can be explained by a van der Waals (vdW) attractive force, as discussed in the literature. In contrast, the film is stable at the hydrophilic quartz (001) surface and the bubble does not attach. Contact angles determined from MD simulations are reported, and these results agree well with experimental and MDS sessile drop results. In this way, film stability and bubble attachment are described with respect to interfacial water structure for surfaces of different polarity. Interfacial water molecules at the hydrophobic molybdenite face surface have relatively weak interactions with the surface when compared to the hydrophilic quartz (001) surface, as revealed by the presence of a 3 Å "water exclusion zone" at the molybdenite/water interface. The molybdenite armchair-edge and zigzag-edge surfaces show a comparably slow process for film rupture and displacement when compared to the molybdenite face surface, which is consistent with their relatively weak hydrophobic character.

Keywords: *Molecular dynamics simulations (MDS), film stability, bubble attachment, interfacial water structure*

1. Introduction

Attachment of air bubbles to mineral particles is of fundamental importance in understanding flotation separation phenomena. It is well known that attachment of an air bubble at a hydrophobic surface includes film thinning, film rupture, and film displacement (Wilson et al., 2000; Somasundaran, 2006). Experimental techniques, including the use of high speed video, can catch the process of bubble attachment at a mineral surface (Drelich and Miller, 2012; Niecikowska et al., 2012). However, molecular scale examination of the phenomena has not yet been reported.

Structural knowledge of interfacial water molecules at mineral surfaces is of significant importance in explaining the hydrophobicity of such surfaces. Different spectroscopic methods have been applied to understand the structures and dynamic properties of interfacial water molecules at mineral surfaces. For example, the water structure at soluble salt surfaces has been studied with Fourier transform infrared spectroscopy (Yalamanchili et al., 1991; Cao et al., 2011; Cheng et al., 2013). Also, vibrational sum-frequency generation spectroscopy has been used to explore the molecular structure of water at oxide mineral surfaces (Shen, 1994; Yeganeh et al., 1999; Ostroverkhov et al., 2005; Shen and Ostroverkhov, 2006) and fluorite surfaces (Eftekhari-Bafrooei and Borguet, 2009; Zhang et al., 2013). However, the spectroscopic signal has been difficult to analyze, and the experimental results require further analysis at the molecular level.

http://dx.doi.org/10.5277/ppmp1821

Because of the marked increase in computational capabilities in recent years, MDS can be used to explore water/mineral interactions and can provide important molecular-level information about the structures and dynamic properties of interfacial water at selected mineral surfaces. Much research based on MDS has been reported on water structure and the dynamic and thermodynamic characteristics of water at mineral surfaces (Lee and Rossky, 1994; Spohr et al., 1999; Rustad, 2001; Gallo et al., 2002; Kalinichev and Kirkpatrick, 2002; Rustad, et al., 2003; Wang et al., 2004; Du and Miller, 2007; Du et al., 2012). Compared to quantum mechanics calculations, MDS has a greater capacity for studying a system with a large number of atoms. Because of this remarkable ability to simulate large systems, the contact angles of nanodrops at solid surfaces can even be measured by MDS (Werder et al., 2003; Jin et al., 2014; Shrimali et al., 2016).

In this study, MDS bubble attachment and contact angles were examined for the first time for the molybdenite face, molybdenite armchair-edge, molybdenite zigzag-edge, and quartz (001) surfaces, and the results are compared to experimental contact angles. In the MD simulations of bubble attachment, there is no gravity nor buoyant force compared to experimental captive bubble contact angle measurements. MDS inter-molecular interactions are represented by Lennard-Jones potentials and electrostatic interactions (Jones, 1924). Of course, the stability of the water film is considered. At the hydrophobic molybdenite surfaces the film is unstable and ruptures, while the water film at the hydrophilic quartz surfaces does not. It is expected for the molybdenite armchair-edge and zigzag-edge surfaces of higher polarity (lower hydrophobicity), that film rupture takes longer than at the molybdenite face surface. In addition, the MDS interfacial water structures are reported to explain wetting characteristics of the surfaces.

2. Methods

2.1 Experimental

Molybdenite crystals were obtained from the rock and mineral collections of the College of Mines and Earth Sciences at the University of Utah. Because of the unique layered structure of molybdenite, in which the MoS_2 layers are held together by van der Waals (vdW) forces, the fresh molybdenite face surfaces were prepared by removing the top MoS_2 layer with adhesive tape. Pure quartz single crystal specimens were purchased from Almaz Optics, Inc. The crystallographic plane for the quartz crystal surface was unknown. The quartz surface was polished to the standard surface quality based on U.S. Standard MIL-PRF-13830B, by Almaz Optics, Inc. The quartz specimen was cleaned by rising with acetone, methanol, and 18 MΩ·cm deionized water obtained from a Milli-Q system. Then, the quartz crystal was blown dry with high-purity nitrogen gas. In order to remove possible organic contamination on the quartz surface, the crystal was treated with argon plasma for 15 minutes.

A Rame-Hart goniometer was used to measure the captive bubble contact angles for selected mineral surfaces. The glass cell used for captive bubble contact angle measurements was cleaned with acetone and methanol then rinsed with 18MΩ·cm deionized water at least three times. The mineral crystal sample was held by two glass cylinders and merged in the glass cell filled with 18MΩ·cm deionized water. Then, beneath the mineral surface an air bubble was released from the needle tip after formation with a syringe. The bubble was captured and attached at the selected mineral surface. Since the contact angle was measured for cases when attachment occurred, contact angles reported in this study are intermediate contact angles, which are between advancing and receding contact angles. At least ten air bubbles were generated and measured for each selected mineral surface. The reported captive bubble contact angle values are the averages of these measurements. The maximum experimental variation in captive bubble contact angle values was found to be ±1°.

2.2 Molecular dynamics simulations

Amber, an MDS program package, was used for the simulation and analysis of bubble attachment and interfacial water at selected mineral surfaces in this study (Pearlman et al., 1995). The total energy is expected to include bonded, Coulombic/electrostatic, and van der Waals interactions, as shown:

$$E_{Total} = E_{bonded} + E_{Coulombic} + E_{vdW}. \quad (1)$$

The bonded term includes the bond stretch and angle bend energy terms. For example, the bond length and angle for the water models are represented as harmonic terms. The Coulombic/electrostatic energy is represented by:

$$E_{Coulombic} = \frac{e^2}{4\pi\epsilon_0}\sum_{i\neq j}\frac{q_i q_j}{r_{ij}} \quad (2)$$

in which the energy of the interaction is inversely proportional to the distance of separation r_{ij}. The terms q_i and q_j are atomic partial charges for atoms i and j. The term e is the charge of an electron, and ϵ_0 is the dielectric permittivity of a vacuum (8.85419×10^{-12} F/m).

The van der Waals energy term, represented by the conventional Lennard-Jones (12-6) function (Jones, 1924), includes the short-range repulsion associated with the increase in energy as two atoms approach each other and the attractive dispersion energy, as is shown:

$$E_{vdW} = \sum_{i\neq j}\varepsilon_{ij}\left[\left(\frac{r_{m,ij}}{r_{ij}}\right)^{12} - 2\left(\frac{r_{m,ij}}{r_{ij}}\right)^{6}\right] \quad (3)$$

where the term ε_{ij} is the depth of the potential well, and $r_{m,ij}$ is the distance at which the potential reaches its minimum.

Interaction parameters between unlike atoms are calculated according to the arithmetic mean rule for the distance parameter, r_m, and the geometric mean rule for the energy parameter, ε:

$$r_{m,ij} = \frac{1}{2(r_{m,i}+r_{m,j})} \quad (4)$$

$$\varepsilon_{ij} = \sqrt{\varepsilon_i \varepsilon_j} \quad (5)$$

The rigid SPC/E water model has the closest average configurational energy to the experimental value (-41.5 KJ mol^{-1}) (Kusalik and Svishchev, 1994; Mahoney and Jorgensen, 2000). Other calculated physical properties of the SPC/E water model are comparable, such as self-diffusion, dielectric constant, and water dipole moment. Thus, the SPC/E water model was selected for exploring the interfacial water at selected mineral surfaces.

The force field model for quartz-SiO_2 is from the CLAYFF force field (Cygan et al., 2004). The Lennard-Jones parameters of molybdenite-MoS_2 are from the Universal Force Field (UFF) (Rappé et al., 1992). Atomic partial charges for the Mo and S atoms in the molybdenite crystal are Mulliken charges determined from the periodic DFT quantum chemical calculations of a well-defined molybdenite-MoS_2 unit cell using the Perdew-Wang 1991 (PW91) functional theory and the generalized gradient approximation (Perdew et al., 1991; Perdew et al., 1996), which is the same approach CLAYFF applied to assign atomic partial charges. The quantum program, DMol3, was used to assign the Mulliken charges (Delley, 2000). The force field parameters for quartz-SiO_2 and molybdenite-MoS_2 are listed in Table 1. The crystal structures for selected minerals in this study are from the American Mineralogist Crystal Structure Database (Downs and Hall-Wallace, 2003). Lattice parameters of the selected minerals are all from X-ray Diffraction (XRD) measurements of natural crystals.

To measure the bubble attachment contact angle of selected mineral surfaces, three steps are required, including creating the selected mineral crystal, simulating a gas bubble in an aqueous phase, and assembling them together in one simulation system. A crystal of the selected mineral with a specific mineral surface exposed was prepared with Crystal Maker software packages (Palmer, 2009). Since periodic conditions are applied in the contact angle simulation, periodic images of the drops were avoided by using mineral surfaces with sufficient surface area. In this simulation, the horizontal extent of the surfaces was about 150 Å × 150 Å. Nitrogen gas was chosen for this simulation. A two point model for nitrogen molecules was used (Rowlinson and Swinton, 2013). The initial coordinates of a nitrogen bubble containing 906 nitrogen molecules in an aqueous phase containing about 100,000 water molecules was generated by the Xleap module of the Amber software packages (Pearlman et al., 1995). Then the isothermal-isobaric (NPT) ensemble was used to run the simulation for equilibration of the water and the nitrogen bubble with a simulation period of 500 ps. The amount (N), pressure (P), and temperature (T) were conserved. The simulation temperature was set as 298 K. After the water box containing the nitrogen bubble reached equilibrium, a portion of the water molecules together with the nitrogen bubble were separated from the initial water box and put adjacent to the selected

mineral crystal surface in another box. The initial distance between the nitrogen bubble and the selected mineral surface was set at 10 Å, i.e. the initial water film thickness at the selected mineral surface is about 10 Å. A simulation period of 1 ns with NVT conditions was used to equilibrate the simulation system, then a subsequent 100 ps simulation was analyzed for measuring the simulated contact angles.

Table 1. Force field parameters for selected minerals

Mineral	Atom	r_m (Å)	ε (Kcal/mol)	q
Quartz-SiO_2	Si	3.7064	0.0000018	2.1
	O	3.5532	0.1554	-1.05
Molybdenite-MoS_2	Mo	3.052	0.056	0.458
	S	4.035	0.274	-0.229

To study the structure and properties of water molecules at selected mineral surfaces, a simulation periodic box was made containing a vacuum space at the top, a water phase in the middle, and a mineral crystal surface at the bottom for each selected mineral. The water box was generated by the Xleap module of the Amber software packages (Pearlman et al., 1995). The mineral crystal was expanded and cut using the CrystalMaker software packages (Palmer, 2009). The dimension of this periodic simulation system was set to about 40 Å × 40 Å × 100 Å. The purpose for having a vacuum space was to make sure the water phase experienced the same pressure for all simulations. After a simulation time of 2 ns for equilibration of the system, a final simulation for another 2 ns was performed to produce results for analysis. The canonical ensemble (NVT) was used for the MD simulations of interfacial water molecules at the selected mineral surfaces, in which case the amount (N), volume (V) and temperature (T) are conserved.

3. Results and discussion

3.1 Film stability and bubble attachment

From snapshots of the MD bubble attachment simulation of selected mineral surfaces, it was difficult to see the nitrogen bubble and visualize its behavior. To have a better view of the simulation, a thin section with thickness of 2 nm in the middle of the simulation periodic box was selected for visualization. Thin sections of the initial (0 ns) and final (1 ns) states are shown by the MDS snapshots presented in Fig. 1, in which the molybdenite, quartz, nitrogen and water molecules are represented by spheres with equal size (0.8 Å). According to the thin sections, nitrogen molecules are dispersed in the gas bubble at a density of 28 g/dm^3, significantly higher than the nitrogen gas density at standard temperature and pressure (1.25 g/dm^3) but still much less than the density of liquid nitrogen at its boiling point (808 g/dm^3).

The Young-Laplace equation for a nitrogen bubble in water is shown in Equation 6, where Δp, γ, and R are the pressure difference across the nitrogen/water interface, the surface tension for water (72.8 dyne/cm at 298 K), and the radius of the bubble, respectively.

$$\Delta p = \frac{2\gamma}{R} \tag{6}$$

According to the Young-Laplace equation, pressure must increase as the bubble size decreases. For the nitrogen bubble with a diameter of 7 nm (R = 3.5 nm) at 298 K, the pressure inside of the bubble is 41.6 × 10^7 dyne/cm^2. A previous study has confirmed this relationship (Takahashi et al., 1979).

At high pressure, the ideal gas law is not valid, so the corrected real gas law at high pressure is applied for the nitrogen bubble, as shown in Equation 7.

$$p(V - nb) = nRT, \tag{7}$$

where V, p, and n are the volume, pressure, and moles of nitrogen. For nitrogen gas the constant b is 0.04 dm^3/mol. T is 298 K, and R is the molar gas constant (8.314 J·K^{-1}·mol^{-1}). Calculation of the number

of molecules in the nitrogen bubble with diameter of 7 nm is 1086, which is close to the number of nitrogen molecules (906) in the MD simulation.

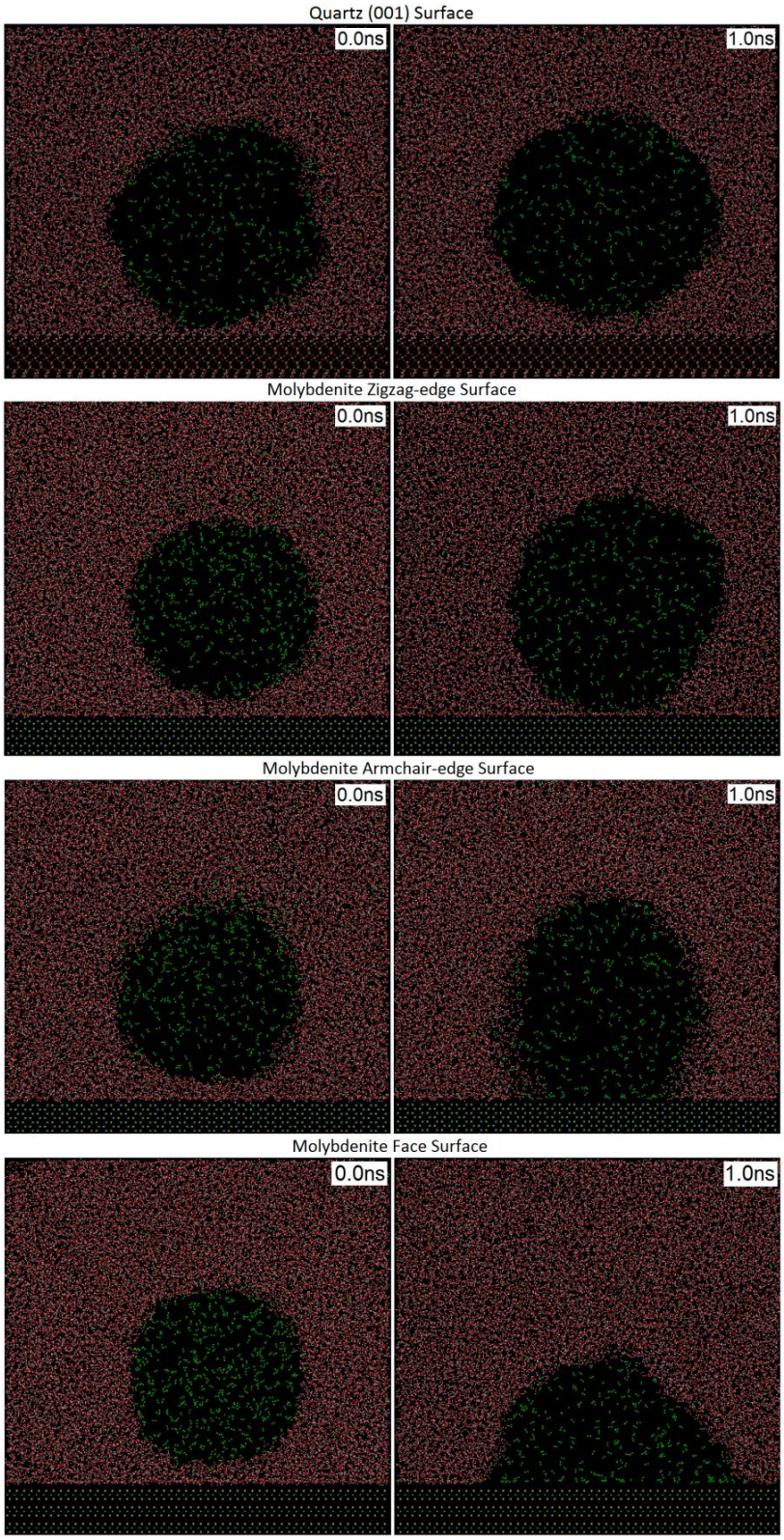

Fig. 1. Thin sections of initial and final states (after 1 ns) of nitrogen bubbles at quartz (001), molybdenite zigzag-edge, molybdenite armchair-edge, and molybdenite face surfaces. The atoms' color codes are as follow: cyan, Mo; green, N; lime, Si; red, O; white, H; yellow, S. Molecular Scale: quartz, 0.8 Å; molybdenite, 0.8 Å; nitrogen, 0.8 Å; water, 0.8 Å

Figure 1 clearly shows that the film between the nitrogen bubble and the quartz surface is stable. Rupture does not occur at the quartz (001) surface, which is consistent with current experimental results and a previous experimental contact angle study of the quartz surface (Subrahmanyam et al., 1999; Kowalczuk et al., 2016). In contrast, for the molybdenite face, armchair-edge, and zigzag-edge surfaces, initially there was a water film about 1 nm thick between the nitrogen gas bubble and the molybdenite crystal surface, but the water film ruptured and the nitrogen gas bubble attached to the molybdenite surface, as shown in Fig. 1. The nitrogen gas bubble at the molybdenite face surface formed a hemisphere. However, at the molybdenite armchair-edge and zigzag-edge surfaces, the nitrogen gas bubble retained a spherical shape (there are even a few water molecules dangling around the bubble attachment area at the molybdenite zigzag-edge surface), which is consistent with their higher polarity when compared to the molybdenite face surface (Jin et al., 2014).

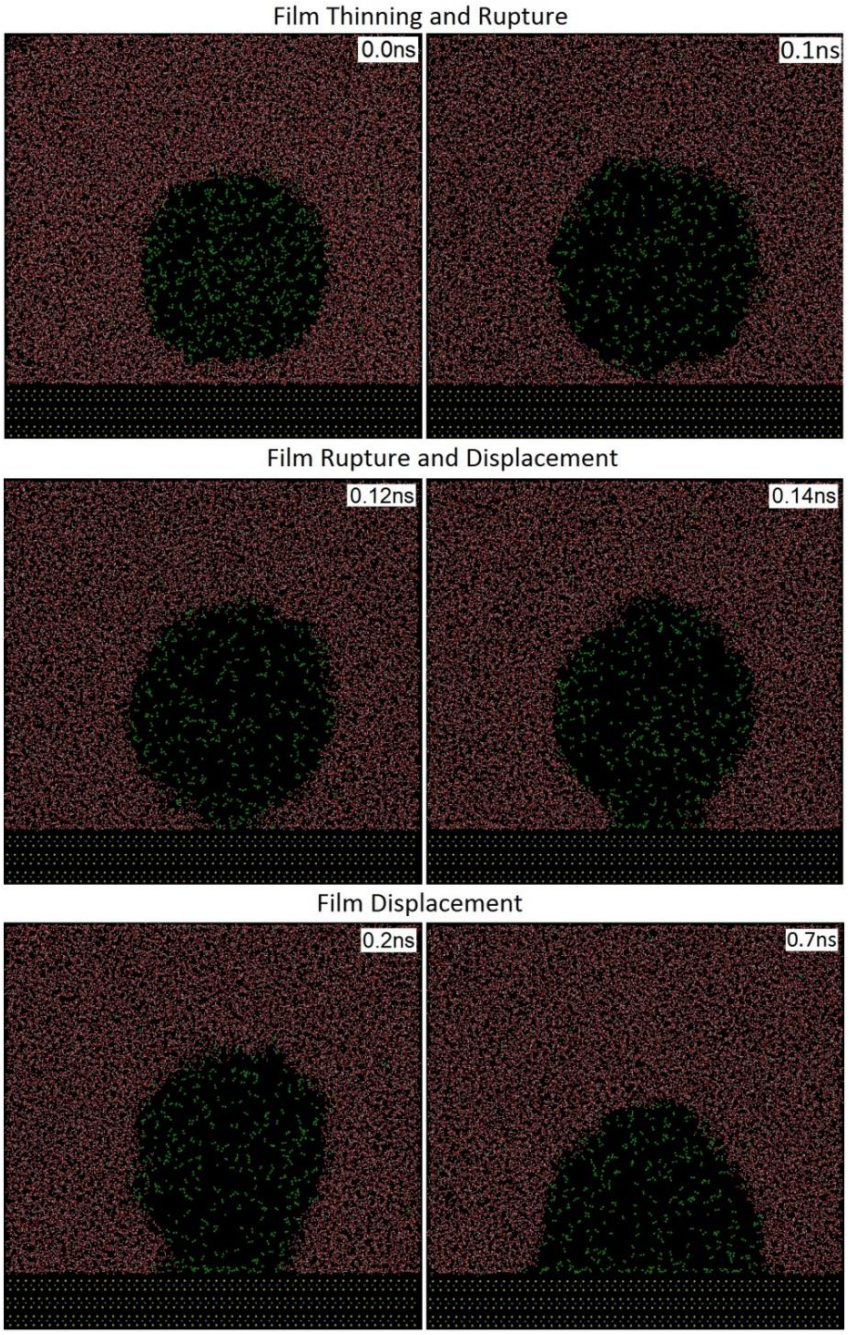

Fig. 2. Thin sections of a nitrogen bubble at a molybdenite face surface showing the process of film thinning, rupture, and displacement. The atoms' color codes are as follow: green, N; cyan, Mo; yellow, S; red, O; white, H. Molecular Scale: molybdenite, 0.8 Å; nitrogen, 0.8 Å; water, 0.8 Å

It is well recognized in the literature that attachment of an air bubble at a hydrophobic surface includes film thinning, film rupture, and film displacement (Wilson et al., 2000; Somasundaran, 2006). MDS results for the attachment of the nitrogen bubble at the molybdenite face surface provide molecular scale information to examine the phenomena reported by previous researchers. Figure 2 shows the process of water film thinning, rupture, and displacement leading to the equilibrium state of attachment (0.7 ns).

The top of Figure 2 shows the process of water film thinning and rupture, in which nitrogen molecules start to reach the molybdenite face surface. The nitrogen molecules diffuse through the water film between the nitrogen bubble and the molybdenite face surface, and reach the molybdenite/water interface. The equivalent diameter of the attachment area is 0.7 nm at 0.1 ns, which corresponds to an attachment area of about 0.4 nm^2. As a result, the gas/solid interface is generated and stabilized, i.e. the film rupture started.

The middle of Figure 2 shows the process of water film rupture and displacement, in which a bridge between the nitrogen bubble and molybdenite face surface is formed. The attachment area at 0.12 ns and 0.14 ns simulation times are 2.1 nm^2 and 7.7 nm^2, respectively. At this point, the film has ruptured, and the attachment area is expanding rapidly, due to film displacement. A nitrogen bridge has formed between the nitrogen bubble and molybdenite face surface.

The bottom of Figure 2 shows further film displacement and the attached nitrogen bubble forms a hemisphere at the molybdenite face surface. More nitrogen molecules rush into the bridge formed as the film is displaced, and the attachment area keeps expanding. Finally (after 1 ns simulation time), the equilibrium state is achieved as indicated by the fact that a hemi-spherical shape of the bubble has been established.

The equivalent diameter of the bubble attachment area for the molybdenite face, armchair-edge, and zigzag-edge surfaces increases with the simulation time, as shown in Fig. 3. The film rupture time can be estimated from MDS and is taken as the time for the equivalent diameter of the bubble attachment area to reach 1 nm. The film rupture times for the molybdenite armchair-edge and zigzag-edge surfaces (between 0.2 and 0.3 ns) are significantly greater than the rupture time for the molybdenite face surface (0.1 ns). After film rupture, film displacement at the molybdenite arm-chair edge surface happened more rapidly than at the molybdenite zigzag-edge surface. At 1 ns, the equivalent bubble attachment area diameters for the molybdenite face, armchair-edge, and zigzag-edge surfaces are 8.3, 6.4, and 2.7 nm, respectively. This is consistent with the difference in the polarity of their surfaces as revealed by water dipole orientation analysis (Jin et al., 2014). The results shown in Fig. 3 suggest that an equilibration state for the bubble at the molybdenite face has been achieved after 1 ns.

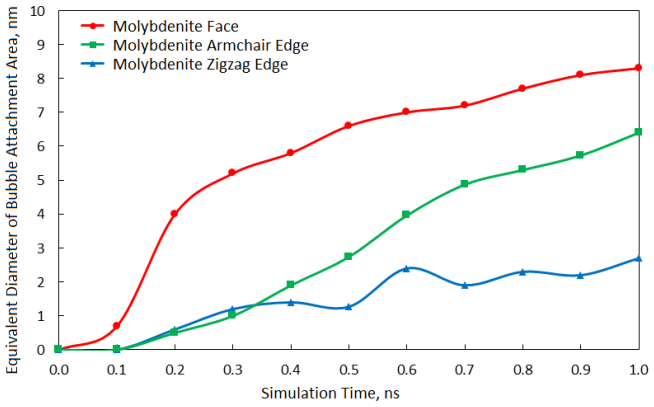

Fig. 3. Variation of equivalent diameter of bubble attachment area with time for the simulation of nitrogen bubble attachment at the molybdenite face, armchair-edge, and zigzag-edge surfaces

3.2 Contact angles

To determine the MDS bubble attachment contact angle, post-processed densities of nitrogen molecules were plotted for two center planes: the x-z plane and the y-z plane. A Fortran program was

applied to calculate the 2-dimensional number densities of nitrogen molecules in the nitrogen gas bubble. The pixel size of this 2-dimensional nitrogen molecule number density calculation is 1Å × 1Å. A two-dimensional air bubble with a contour line corresponding to the lowest nitrogen density defines the boundary of the nitrogen gas bubble, and the results were expressed as a best fit contour line. For each bubble attachment contact angle measurement, the contact angles were measured in the x-z and y-z planes and then averaged.

The spherical shape of the established nitrogen bubble at the quartz (001) surface after 1 ns simulation time, as shown in Fig. 1, is consistent with the experimental captive bubble measurements at the quartz surface, in which film rupture does not occur. Thus, both the MDS bubble attachment and experimental captive bubble contact angles at the quartz (001) surface are 0^o. However, in MD simulations there is no gravity, nor buoyant force, so the MDS bubble attachment contact angles are only influenced by the interatomic electrostatic and vdW interactions. The thickness of the water film at the quartz (001) surface is around 1 nm, which is much thinner than the experimental value of 100 nm reported in the literature (Wang et al., 2015). The cut-off distance in this simulation is set at 1 nm, i.e. the interaction between two atoms over 1nm distance is not calculated. This cut-off distance is an empirical value validated for MDS studies of intermolecular interactions (Dang and Smith, 1995). In MD simulation if two molecules are over 1 nm from each other after reaching equilibrium, the intermolecular interactions should be very weak. Thus, the MDS water film thickness at the quartz (001) surface indicates the very weak interaction between the nitrogen bubble and the quartz (001) surface. The MDS and experimental sessile drop contact angles of the quartz (001) surface are 9° and 5° respectively, as presented in Table 2, which are consistent with MDS bubble attachment and experimental captive bubble contact angles (Jin, 2016).

Table 2. MDS and experimental contact angles for molybdentie face, armchair-edge, zigzag-edge, and quartz (001) surfaces

Mineral Surface	Contact Angle, degree			
	Bubble Attachment		Sessile Drop	
	MDS	Experimental	MDS	Experimental
Quartz (001) Surface	0	0 (random surface)	9	5
Molybdenite Zigzag-edge Surface	45	-	24	36
Molybdenite Armchair-edge Surface	65	-	54	
Molybdenite face Surface	90	75	84	85

The experimental captive bubble (air) contact angle at the molybdenite face surface prepared by the procedures provided in this study is 75^o, which is consistent with a previous study (Beaussart et al., 2012). According to the height (about 45Å) and width (about 95Å) of the nitrogen bubble in the 2-dimensional density plot, the shape of the nitrogen bubble attached at the molybdenite face surface is close to a hemisphere, which confirms the thin section snapshot shown in Fig. 1. By drawing a circle at the edge of the nitrogen bubble and a tangential line at the three-phase line of contact, a contact angle of about 90^o can be measured. The MDS bubble attachment contact angle for the molybdenite face surface is very close to the MDS and experimental sessile drop contact angle results (84° and 85°) but slightly larger than the corresponding experimental captive bubble contact angle. See Table 2. The significance of gas phase composition has not been considered. Values of the MDS bubble attachment contact angles for the two molybdenite edge surfaces are between the contact angles of the molybdenite face and quartz (001) surfaces, which is consistent with the MDS and experimental sessile drop contact angles, indicating a relatively modest hydrophobic surface character. The molybdenite zigzag-edge surface has relatively smaller MDS bubble attachment and sessile drop contact angles when compared to the armchair-edge surface, which reveals a stronger interaction between the zigzag-edge surface with interfacial water molecules. The two point model for nitrogen molecules used in this simulation may need further improvement to simulate the nitrogen bubble attachment by MDS. A three point model for nitrogen molecules will be used in future MDS bubble attachment studies (Somasundaram et al., 1999).

3.3 Interfacial water analysis

In the analysis of the number density distribution of interfacial water molecules at the selected mineral surfaces, the simulation periodic box was divided into 0.5 Å bins parallel to the selected surface. The number of molecules or ions in each bin was counted. In this study, the position of a water molecule is defined as the position of the center of mass for the water molecule. The number of molecules in each bin was plotted versus the bin's distance from the surface, making the number density profile. The position of the selected mineral surface is defined as the position of the top layer of atoms.

According to the water number density profile for the molybdenite face surface shown in Figure 4, the first water density peak is about 3.5 Å away from the surface, and this distance is greater than the distance between hydrogen-bonded water/water molecules, which is approximately 2.8 Å (Abraham, 1978; Dang and Pettitt, 1990; Rasaiah and Zhu, 1990; Smith and Dang, 1994; Lynden-Bell and Rasaiah, 1997). This result is consistent with the "water exclusion zone" presented in the snapshot of the molybdenite/water interface in Fig. 4 and demonstrates the relatively weak interaction between the interfacial water molecules and molybdenite face surface. This "water exclusion zone" is filled with possible electron orbitals from water and from the crystal surface, and its thickness is the distance between the center of the surface atoms and the center of mass for interfacial water molecules. This spontaneous attachment can be explained by a van der Waals attractive force as discussed in the literature (Wang et al., 2015). In contrast, the "water exclusion zone" is not present at the quartz (001) surface, which is consistent with a previous MDS study (Wang et al., 2006). Thus, compared to the hydrophobic molybdenite face surface, the interfacial water molecules at the quartz (001) surface have much stronger interactions with the surface. According to the snapshot shown in Figure 4, water molecules in the first water layer are highly ordered and form hydrogen bonds with oxygen atoms at the quartz (001) surface, and the water molecules in the second water layer form hydrogen bonds with the first water layer. As a result, in MD bubble attachment simulation for the molybdenite face surface, the nitrogen molecules were able to reach the molybdenite face surface resulting in film rupture, while for the quartz (001) surface, the nitrogen molecules couldn't penetrate the water film hydrogen bonded with the surface oxygen atoms, and the film didn't break. The "water exclusion zone" at the molybdenite armchair-edge and zigzag-edge surfaces (both about 3 Å) are relatively smaller than at the molybdenite face surface, which is consistent with the relatively strong interaction between these surfaces and interfacial water molecules (Jin et al., 2014). As a result, film rupture time at the molybdenite armchair-edge and zigzag-edge surfaces is longer than at the molybdenite face surface.

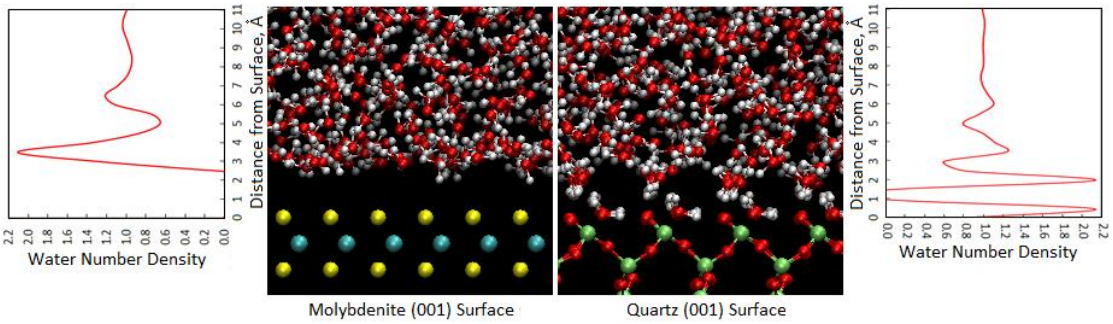

Fig. 4. MDS snapshots and water number density profiles of molybdenite/water (left) and quartz/water (right) interfaces. The simulation time is 2 ns. The atoms' color codes are as follow: cyan, Mo; lime, Si; green, Al; red, O; white, H in water; pink, H in OH group; yellow, S

For the SPC/E water model, two water molecules are defined as hydrogen bonded if the distance between the two oxygen atoms is less than 3.5 Å and the O…O-H angle is simultaneously less than 30° (Luzar and Chandler, 1996). The hydrogen bonding between a surface oxide and a water molecule is defined in the same way as the hydrogen bonding between two water molecules. Distribution of the average number of hydrogen bonds per water molecule along the surface normal for the molybdenite and quartz (001) surfaces are shown in Figure 5. The total number of hydrogen bonds per water

molecule includes both the hydrogen bonding with adjacent water molecules and with the oxygen atoms from the quartz (001) surface. The number of hydrogen bonds per water of the bulk water molecules about 1 nm from the surface is around 3.35, which confirms the value of 3.5 from the previous MDS study (Nieto-Draghi et al., 2003). Due to the lack of hydrogen bonding donors at the hydrophobic molybdenite face surface, the interfacial water molecules have only approximately half of the hydrogen bonds per water molecule compared to the bulk water. However, because of the contribution from the oxygen atoms at the quartz (001) surface, the first layer water molecules at the quartz (001) surface have a total of 4.7 hydrogen bonds per water, which is consistent with the previous study (Wang et al., 2012). Results of the hydrogen bonding analysis support the MDS snapshots and water number density profiles.

In addition to the structural properties, the dynamic properties, such as water residence time, for the interfacial water molecules at selected mineral surfaces can be studied using MDS. The water residence time is described as the time a water molecule spends in each water layer along the surface. It has been calculated using the residence-time correlation functions (Berendsen et al., 1987; Koneshan et al., 1998; Chowdhuri and Chandra, 2001;). The water residence time at the hydrophilic quartz (001) surface is 44 ps, which is much larger than the water residence time at the hydrophobic molybdenite face surface (8 ps) (Jin et al., 2014). This is consistent with the fact that interfacial water molecules form hydrogen bonds with the oxygen atoms on the hydrophilic quartz (001) surface, while the interfacial water molecules have relatively weak interactions with the hydrophobic molybdenite face surface. The water residence times at the molybdenite armchair-edge and zigzag-edge surfaces are 9 and 10.5 ps, which are significantly longer than the water residence time at the molybdenite face surface (8 ps). This is consistent with their relatively stronger interaction with the interfacial water molecules and higher polarity of these surfaces.

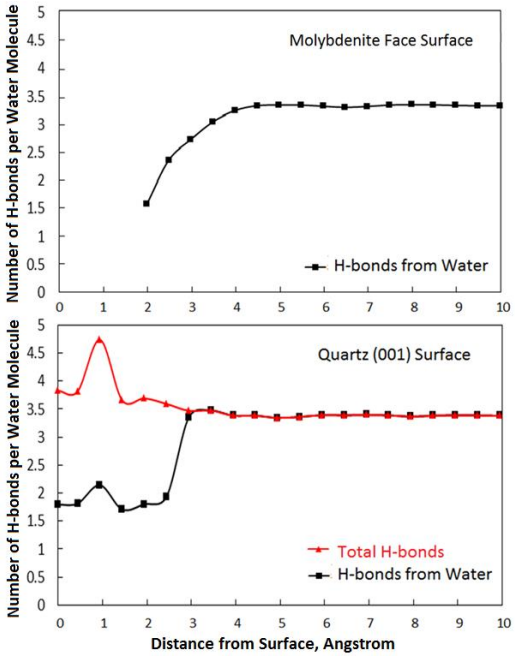

Fig. 5. Distribution of hydrogen-bonding number per water molecule along the surface normal for molybdenite face surface (top) and quartz (001) surface (bottom)

4. Conclusions

According to film stability and bubble attachment MD simulations, film rupture does not occur at the hydrophilic quartz surface, whereas film rupture and bubble attachment do occur at the hydrophobic molybdenite face surface, and a contact angle is established. The film thinning, film rupture, and film displacement processes during bubble attachment at the molybdenite face surface have been explored with MDS. The MDS contact angles at the molybdenite face surface and at the quartz surface are consistent with experimental results. The film rupture times for the molybdenite armchair-edge and

zigzag-edge surfaces are relatively longer than for the molybdenite face surface. Also, the film displacement times for the molybdenite edge surfaces are comparably slower, and simulation time should be extended to reach equilibrium.

MDS interfacial water analysis shows relatively weak interaction between the interfacial water molecules and the hydrophobic molybdenite face surface, which accounts for the presence of a "water exclusion zone" at such hydrophobic surfaces and explains spontaneous bubble attachment due to an attractive van der Waals force (Wang et al., 2015). On the other hand, the hydrogen bonding interaction between the interfacial water molecules and the surface oxygen atoms accounts for the film stability at the hydrophilic quartz (001) surface. The relatively stronger interaction between interfacial water molecules and the molybdenite edge surfaces is consistent with their modest hydrophobic character.

Acknowledgements

This work was funded by the Division of Chemical Sciences, Geosciences, and Biosciences, Office of Basic Energy Sciences (BES) of the U.S. Department of Energy through Grant No. DE-FG-03-93ER14315. The support and resources from the Center for High Performance Computing at the University of Utah are gratefully acknowledged. Part of the calculations were carried out using computer resources provided by the Division of Chemical Sciences, Geosciences, and Biosciences, Office of Basic Energy Sciences (BES), of the DOE at the Pacific Northwest National Laboratory.

References

ABRAHAM, F. F., 1978. *The interfacial density profile of a Lennard-Jones fluid in contact with a (100) Lennard-Jones wall and its relationship to idealized fluid/wall systems: A Monte Carlo simulation.* The Journal of Chemical Physics, 68(8), 3713-3716.

BEAUSSART, A., PARKINSON, L., MIERCZYNSKA-VASILEV, A., BEATTIE, D. A., 2012. *Adsorption of modified dextrins on molybdenite: AFM imaging, contact angle, and flotation studies.* Journal of Colloid and Interface Science, 368(1), 608-615.

BERENDSEN, H., GRIGERA, J., STRAATSMA, T., 1987. *The missing term in effective pair potentials*. Journal of Physical Chemistry, 91(24), 6269-6271.

CAO, Q., WANG, X., MILLER, J. D., CHENG, F., JIAO, Y., 2011. *Bubble attachment time and FTIR analysis of water structure in the flotation of sylvite, bischofite and carnallite*. Minerals Engineering, 24(2), 108-114.

CHENG, F., CAO, Q., GUAN, Y., CHENG, H., WANG, X., MILLER, J. D., 2013. *FTIR analysis of water structure and its influence on the flotation of arcanite (K_2SO_4) and epsomite ($MgSO_4 \cdot 7H_2O$).* International Journal of Mineral Processing, 122, 36-42.

CHOWDHURI, S., CHANDRA, A., 2001. *Molecular dynamics simulations of aqueous NaCl and KCl solutions: Effects of ion concentration on the single-particle, pair, and collective dynamical properties of ions and water molecules.* The Journal of Chemical Physics, 115, 3732.

CYGAN, R. T., LIANG, J.-J., KALINICHEV, A. G., 2004. *Molecular models of hydroxide, oxyhydroxide, and clay phases and the development of a general force field*. The Journal of Physical Chemistry B, 108(4), 1255-1266.

DANG, L. X., PETTITT, B. M., 1990. *A theoretical study of like ion pairs in solution*. Journal of Physical Chemistry, 94(10), 4303-4308.

DANG, L. X., SMITH, D. E., 1995. *Comment on ''Mean force potential for the calcium–chloride ion pair in water'' [J. Chem. Phys. 99, 4229 (1993)].* The Journal of Chemical Physics, 102(8), 3483-3484.

DELLEY, B., 2000. *DMol3 DFT studies: from molecules and molecular environments to surfaces and solids.* Computational Materials Science, 17(2), 122-126.

DOWNS, R. T., HALL-WALLACE, M., 2003. *The American Mineralogist crystal structure database.* American Mineralogist, 88(1), 247-250.

DRELICH, J., MILLER, J. D., 2012. *Induction time measurements for air bubbles on chalcopyrite, bornite, and gold in seawater.* Water in Mineral Processing, Proceedings of the First International Symposium, J. Drelich (ed.), Society for Mining, Metallurgy, and Exploration (SME) Englewood, CO, USA, 73-85.

DU, H., MILLER, J., 2007. *A molecular dynamics simulation study of water structure and adsorption states at talc surfaces.* International Journal of Mineral Processing, 84(1), 172-184.

DU, H., YIN, X., OZDEMIR, O., LIU, J., WANG, X., ZHENG, S., MILLER, J.D., 2012. *Molecular dynamics simulation analysis of solutions and surfaces in nonsulfide flotation systems.* In: Molecular Modeling for the Design of Novel Performance Chemicals and Materials, B. Rai (ed.), CRC Press, Boca Raton, FL, USA, Chapter 4.

EFTEKHARI-BAFROOEI, A., BORGUET, E., 2009. *Effect of surface charge on the vibrational dynamics of interfacial water*. Journal of the American Chemical Society, 131(34), 12034-12035.

GALLO, P., RAPINESI, M., ROVERE, M., 2002. *Confined water in the low hydration regime.* The Journal of Chemical Physics, 117, 369.

JIN, J., 2016. *Wetting and Interfacial Water Analysis of Selected Mineral Surfaces as Determined by MDS and SFVS.* PhD Dissertation, University of Utah, Salt Lake City, UT, USA.

JIN, J., MILLER, J. D., DANG, L. X., 2014. *Molecular dynamics simulation and analysis of interfacial water at selected sulfide mineral surfaces under anaerobic conditions.* International Journal of Mineral Processing, 128, 55-67.

JONES, J. E., 1924. *On the determination of molecular fields. I. From the variation of the viscosity of a gas with temperature*. Paper presented at the Proceedings of the Royal Society of London A: Mathematical, Physical and Engineering Sciences, 106, 441-462.

KALINICHEV, A. G., KIRKPATRICK, R. J., 2002. *Molecular dynamics modeling of chloride binding to the surfaces of calcium hydroxide, hydrated calcium aluminate, and calcium silicate phases*. Chemistry of Materials, 14(8), 3539-3549.

KONESHAN, S., RASAIAH, J. C., LYNDEN-BELL, R., LEE, S., 1998. *Solvent structure, dynamics, and ion mobility in aqueous solutions at 25 C*. The Journal of Physical Chemistry B, 102(21), 4193-4204.

KOWALCZUK, P.B., ZAWALA, J., DRZYMALA, J., MALYSA, K., 2016. *Influence of hexylamine on kinetics of flotation and bubble attachment to the quartz surface.* Separation Science and Technology, 51(15-16), 2681-2690.

KUSALIK, P. G., SVISHCHEV, I. M., 1994. *The spatial structure in liquid water*. Science, 265(5176), 1219-1221.

LEE, S. H., ROSSKY, P. J., 1994. *A comparison of the structure and dynamics of liquid water at hydrophobic and hydrophilic surfaces – a molecular dynamics simulation study*. The Journal of Chemical Physics, 100, 3334.

LUZAR, A., CHANDLER, D., 1996. *Effect of environment on hydrogen bond dynamics in liquid water.* Physical Review Letters, 76(6), 928.

LYNDEN-BELL, R., RASAIAH, J., 1997. *From hydrophobic to hydrophilic behaviour: A simulation study of solvation entropy and free energy of simple solutes.* The Journal of Chemical Physics, 107(6), 1981-1991.

MAHONEY, M. W., JORGENSEN, W. L., 2000. *A five-site model for liquid water and the reproduction of the density anomaly by rigid, nonpolarizable potential functions.* The Journal of Chemical Physics, 112(20), 8910-8922.

NIECIKOWSKA, A., KRASOWSKA, M., RALSTON, J., MALYSA, K., 2012. *Role of surface charge and hydrophobicity in the three-phase contact formation and wetting film stability under dynamic conditions.* The Journal of Physical Chemistry C, 116(4), 3071-3078.

NIETO-DRAGHI, C., ÁVALOS, J. B., ROUSSEAU, B., 2003. *Transport properties of dimethyl sulfoxide aqueous solutions.* The Journal of Chemical Physics, 119(9), 4782-4789.

OSTROVERKHOV, V., WAYCHUNAS, G. A., SHEN, Y., 2005. *New information on water interfacial structure revealed by phase-sensitive surface spectroscopy*. Physical Review Letters, 94(4), 046102.

PALMER, D., 2009. *CrystalMaker Software:* CrystalMaker Software Ltd, Oxford, England.

PEARLMAN, D. A., CASE, D. A., CALDWELL, J. W., ROSS, W. S., CHEATHAM, T. E., DEBOLT, S., KOLLMAN, P., 1995. *AMBER, a package of computer programs for applying molecular mechanics, normal mode analysis, molecular dynamics and free energy calculations to simulate the structural and energetic properties of molecules*. Computer Physics Communications, 91(1), 1-41.

PERDEW, J. P., BURKE, K., ERNZERHOF, M., 1996. *Generalized gradient approximation made simple.* Physical Review Letters, 77(18), 3865.

PERDEW, J. P., ZIESCHE, P., ESCHRIG, H., 1991. *Electronic structure of solids' 91 (Vol. 11):* Akademie Verlag, Berlin.

RAPPÉ, A. K., CASEWIT, C. J., COLWELL, K., GODDARD III, W., SKIFF, W., 1992. *UFF, a full periodic table force field for molecular mechanics and molecular dynamics simulations.* Journal of the American Chemical Society, 114(25), 10024-10035.

RASAIAH, J. C., ZHU, J., 1990. *Cavity functions and association in models for weak electrolytes and sticky hard spheres.* The Journal of Chemical Physics, 92(12), 7554-7564.

ROWLINSON, J. S., SWINTON, F., 2013. *Liquids and Liquid Mixtures: Butterworths Monographs in Chemistry:* Butterworth-Heinemann, London, UK.

RUSTAD, J. R., 2001. *Molecular models of surface relaxation, hydroxylation, and surface charging at oxide-water interfaces*. Reviews in Mineralogy and Geochemistry, 42(1), 169-198.

RUSTAD, J. R., FELMY, A. R., BYLASKA, E. J., 2003. *Molecular simulation of the magnetite-water interface.* Geochimica et Cosmochimica Acta, 67(5), 1001-1016.

SHEN, Y., 1994. *Surfaces probed by nonlinear optics.* Surface Science, 299, 551-562.

SHEN, Y. R., OSTROVERKHOV, V., 2006. *Sum-frequency vibrational spectroscopy on water interfaces: Polar orientation of water molecules at interfaces*. Chemical Reviews, 106(4), 1140-1154.

SHRIMALI, K., JIN, J., VAZIRI HASSAS, B., WANG, X., MILLER, J.D., 2016. *The surface state of hematite and its wetting characteristics.* Journal of Colloid and Interface Science, 477, 16-24.

SMITH, D. E., DANG, L. X., 1994. *Computer simulations of NaCl association in polarizable water.* The Journal of Chemical Physics, 100(5), 3757-3766.

SOMASUNDARAM, T., LYNDEN-BELL, R., PATTERSON, C., 1999. *A simulation study of the kinetics of passage of CO_2 and N_2 through the liquid/vapor interface of water.* The Journal of Chemical Physics, 111(5), 2190-2199.

SOMASUNDARAN, P., 2006. *Encyclopedia of surface and colloid science (Vol. 1):* CRC press, Boca Raton, FL, USA.

SPOHR, E., HARTNIG, C., GALLO, P., ROVERE, M., 1999. *Water in porous glasses. A computer simulation study.* Journal of Molecular Liquids, 80(2), 165-178.

SUBRAHMANYAM, T., MONTE, M., MIDDEA, A., VALDIVIEZO, E., LINS, F., 1999. *Contact angles of quartz by capillary penetration of liquids and captive bubble techniques.* Minerals Engineering, 12(11), 1347-1357.

TAKAHASHI, T., MIYAHARA, T., MOCHIZUKI, H., 1979. *Fundamental study of bubble formation in dissolved air pressure flotation.* Journal of Chemical Engineering of Japan, 12(4), 275-280.

WANG, J., KALINICHEV, A. G., KIRKPATRICK, R. J., 2004. *Molecular modeling of water structure in nano-pores between brucite (001) surfaces.* Geochimica et Cosmochimica Acta, 68(16), 3351-3365.

WANG, J., KALINICHEV, A. G., KIRKPATRICK, R. J., 2006. *Effects of substrate structure and composition on the structure, dynamics, and energetics of water at mineral surfaces: A molecular dynamics modeling study.* Geochimica et Cosmochimica Acta, 70(3), 562-582.

WANG, X., YIN, X., NALASKOWSKI, J., DU, H., MILLER, J., 2012. *Molecular features of water films created with bubbles at hydrophilic and hydrophobic surfaces*. Proceedings XXVI International Mineral Processing Congress, IMPC 2012, New Delhi, India, 5819-5828.

WANG, X., YIN, X., NALASKOWSKI, J., DU, H., MILLER, J. D., 2015. *Molecular features of water films created with bubbles at silica surfaces*. Surface Innovations, 3(SI1), 20-26.

WERDER, T., WALTHER, J. H., JAFFE, R., HALICIOGLU, T., KOUMOUTSAKOS, P., 2003. *On the water-carbon interaction for use in molecular dynamics simulations of graphite and carbon nanotubes.* The Journal of Physical Chemistry B, 107(6), 1345-1352.

WILSON, I. D., ADLARD, E. R., COOKE, M., POOLE, C. F., 2000. *Encyclopedia of Separation science,* Academic Press, San Diego, CA, USA.

YALAMANCHILI, M., KELLAR, J., MILLER, J., 1991. I*n-situ FT-IR internal reflection spectroscopy of collector adsorption phenomena in soluble-salt flotation systems.* Paper presented at the Proceedings of the XVII International Mineral Processing Congress., Dresden, Germany, 23-28 September 1991.

YEGANEH, M., DOUGAL, S., PINK, H., 1999. *Vibrational spectroscopy of water at liquid/solid interfaces: Crossing the isoelectric point of a solid surface.* Physical Review Letters, 83(6), 1179.

ZHANG, X., DU, H., WANG, X., MILLER, J., 2013. *Surface chemistry considerations in the flotation of rare-earth and other semisoluble salt minerals.* Minerals & Metallurgical Processing, 30(1) 24-37.